Amphiphilic Phenyl−Ethynylene Polymers and Copolymers. Synthesis, Characterization, and Optical Emission Properties

E. Arias-Marin,[†,§] J. Le Moigne,*[,†] T. Maillou,[†] D. Guillon,[†] I. Moggio,[†,§] and B. Geffroy[‡]

Institut de Physique et Chimie des Matériaux de Strasbourg, UMR 7504, 23 rue du Loess BP 43, 67034 Strasbourg, France, and LETI (CEA Technologies Avancées), DEIN/SPE, Groupe Composants Organiques, CEA Saclay, 91191 Gif-sur-Yvette Cedex, France

Received January 23, 2002; Revised Manuscript Received March 3, 2003

ABSTRACT: A series of new rigid amphiphilic aryl−ethynylene homopolymers and copolymers with phenyl, pyridinyl, thionyl, or carbazolyl as aryl units has been synthesized. A single side chain on the phenyl rings (alkyl−hydroxyl ester group) provides an amphiphilic character to the polymer backbone. The polymers are characterized by NMR, elemental analysis and size exclusion chromatography (SEC); the thermal properties are analyzed by TGA, DSC, and X-ray diffraction. The polymers with side chains are enough amphiphilic to give stable Langmuir films on water, and the LB films can be transferred on hydrophilic or hydrophobic substrates. The films are deposited on treated glass or silicon substrate. Analyzed by grazing incidence X-ray analysis (GIXA) and by atomic force microscopy (AFM), they reveal well-structured layering periods of 3.5 and 2.7−2.9 nm for the phenyl homopolymer (pPE*n*Bz) and the copolymers with pyridine (pPE*n*(Bz-*co*-Py)) and thiophene (pPE*n*(Bz-*co*-Ti)), respectively. These results suggest a rearrangement in a Y-type bilayer for the pPE*n*Bz on a hydrophilic substrate. For copolymers pPE*n*(Bz-*co*-Py), and pPE*n*(Bz-*co*-Ti), deposited on a hydrophobic substrate, the self-assembly within one layer consists of interdigitated alkyl chains. In solid-state films the polymers and copolymers show a rather good photoluminescence yield and large Stokes-shifts with emission peaks at 539, 502, 569, and 563 nm for pPE*n*Bz, pPE*n*(Bz-*co*-Py), pPE*n*(Bz-*co*-Ti), and pPE*n*(Bz-*co*-Cz), respectively. The photoluminescence quantum yields are decreasing in the series by 23, 15, 12, and 7% respectively, while no emission is observed from pPE*n*Py. A dichroism on LB films has been found in absorption (R = 2.0, 2.04 and 1.3) and in emission spectra (R = 3.4, 4.0 and 2.6) for pPE*n*Bz, pPE*n*(Bz-*co*-Ti) and pPE*n*(Bz-*co*-Py), respectively. LED properties are demonstrated using the ITO/polymer/LiF−Al sandwich, yielding photon emission at 555 and 550 nm for pPE*n*Bz and pPE*n*(Bz-*co*-Py). These results are very important for the future realization by LB deposition technique of more sophisticated devices for polarized emission with further enhanced brightness and improved light efficiency.

1. Introduction

It is now well recognized that the unique electrical and optical properties of conjugated polymers are of great importance for modern technology[1]. Indeed many applications have been recently reported for conjugated polymers in waveguides,[2,3] fluorescent chemical sensors,[4] photoconductors,[5] organic light-emitting diodes (OLEDs),[6−8] etc. The basic characteristics, required for conjugated materials in OLEDs, are semiconducting properties and high quantum yield of the photoluminescence. Moreover, attracting properties of polymers such as the tunable emission wavelengths in a wide range of color and a good solubility, which are required for a low cost manufacturing, are of great interest. These properties are the privileged domains of chemists, who can modify widely the spectral range of emission by inserting specific electroactive substituents[9] as well as enhance the usually poor solubility of the rigid conjugated backbone by grafting flexible chains to the polymer backbone.[10] Even when these requirements are achieved, it is necessary, however, to optimize the quality of the emitting layer by an appropriate deposition technique, to control the film morphology, the carrier mobility and the emission yield of the device. In this respect, the Langmuir−Blodgett (LB) is a promising technique that provides self-organized systems[11] with good molecular order and molecular alignment, indispensable features to obtain polarized light.[12,13]

We recently reported[7,14] on the preparation and characterization of LB films of a series of oligomers based on the phenyl−ethynylene unit (oPE*n*). We observed high electroluminescent and photoluminescent properties for the longest molecules with $n \geq 5$.[7,15] The heptamer gives rise to well oriented films by LB uniaxial compression or mechanical rubbing and polarized light in an emitting diode was successfully obtained.[15] Following our first investigations on these series of phenyl−ethynylene materials, we report here on the macromolecular and the electrooptical properties of polymers and aryl copolymers of benzoate ethynylene. The alternating aryl units are pyridine or carbazole as electron acceptors; or thiophene as electron donor, which are able to tailor the emission properties of the active layer. The present work concerns the synthesis, the polymer characterization, and the spectroscopic properties of homopolymers (benzoate or pyridine) and copolymers (benzoate-*co*-pyridine, benzoate-*co*-carbazole, and benzoate-*co*-thiophene) and their deposition in LB films. In addition, preliminary data concerning the intrinsic electroluminescent properties of spin-coated films of pPE*n*Bz and the copolymer pPE*n*(Bz-*co*-Py) are here presented. The good optical quality obtained with the LB films, with emissions ranging from the blue-green

[†] Institut de Physique et Chimie des Matériaux de Strasbourg, UMR 7504.
[‡] CEA Saclay.
[§] Present address CIQA, Blvd. Enrique Reyna 140, 25100 Saltillo, México.

10.1021/ma020121e CCC: $25.00
Published on Web 04/24/2003

Scheme 1. Pd/Cu Cross Coupling Reaction for the Synthesis of the Homo- and Copolymers Studied in This Work[a]

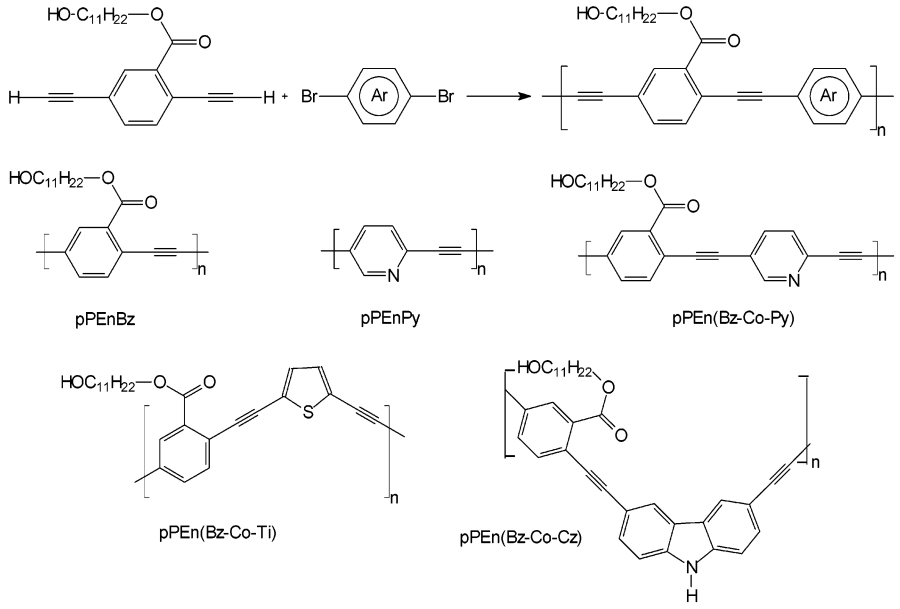

[a] Ar can be (11-undecanol) 2,5-dibromobenzoate, 2,5-dibromopyridine, 3,6-dibromocarbazole, or 2,5-dibromothiophene. The lateral chains (11-undecanol) substituted on the benzoate rings improve the solubility and the amphiphilic character of the molecule.

to the yellow region, and the good molecular orientation achieved could be promising features to obtain polarized light in LED devices.

2. Results and Discussion

2.1. Polymer Synthesis and Characterization. The series of homopolymers and copolymers have been synthesized according to the chemical route given in the literature.[16] Scheme 1 shows the chemical formula of such poly(aryl−ethynylene) homopolymers and copolymers studied in this work. The benzoate, pyridine, benzoate−pyridine, benzoate−thiophene and benzoate−carbazole derivatives are hereafter named pPE*n*Bz, pPE*n*Py, pPE*n*(Bz-*co*-Py), pPE*n*(Bz-*co*-Ti), and pPE*n*(Bz-*co*-Cz), respectively. Some specific synthesis details are reported in the Experimental Part. The long side chain (11-undecanol) grafted on the benzoate moiety improves the solubility and introduces an amphiphilic character to the materials through the hydroxyl groups. For all these materials, Tables 1a and b give the determination by SEC, the average molecular weight ($M_{w(PSeq)}$), relative to the polystyrene (PS) or relative to the oligomer calibration ($M_{w(oPEneq)}$), the weight-average degree of polymerization $\overline{DP}_w$, the polydispersity index (M_w/M_n) and the mean chain length ($\bar{L}_g$), respectively. Figure 1 shows the PS calibration and the specific calibration obtained with the homologous oligomers oPE*n*Bz having 1, 2, 3, 5, and 7 repeat units.[7,17] $\overline{DP}_w$ and $\bar{L}_g$ are calculated from $\bar{M}_{w(oPEneq)}$. Indeed several authors such as Giesa[18] and Tour[19] have already highlighted that the molecular weights calculated from PS standards are not reliable for rigid rod polymers. Size exclusion chromatography (SEC) affords the measurements of the hydrodynamic volumes of macromolecules, which are greatly different for a rigid rod chain and a random coil of a PS chain. From the present experimental data, it can be seen how the molecular weight of the rigid rod aryl−ethynylene polymers can be strongly overestimated and directly affected by the number of alkyl chains substituted on the aromatic rings. This overestimation is more evident at low molecular weights, while according to the ($M_{w(oPEneq)}$) calibration curve, the tendency for higher M_w seems to have a better correlation with those obtained with the PS calibration curve. The homopolymer pPE*n*Bz, bearing the (11-undecanol) benzoate group per phenyl unit shows the highest $\bar{M}_{w(oPEneq)} \approx 3880$ Da, while the unsubstituted pyridine derivative, pPE*n*Py, is only 1014 Da. Similar results were already reported for oligo(aryl−ethynylene)s in the pioneer work of Sanechika et al.[20] A drastic increase of the molecular weight M_w can be observed in the coupling reaction by using a cosolvent to triethylamine, i.e., THF (5% v/v). In these conditions $\bar{M}_{w(oPEneq)}$ rises to 7887; $\overline{DP}_w$, 25 while $\bar{M}_{w(PSeq)} = 33\,600$. However, the polymerization yield is much lower (75%); this decrease is due

Table 1. (a) SEC Results of the Oligomers oPE*n* Used To Build a Calibration Curve from Their Actual Molecular Weight and Their Calculated Elution and Volume (V_e) in THF and (b) Comparative Molecular Weights of Homo and Copolymers Obtained by Both the Polystyrene Calibration Curve ($M_{w(PSeq)}$) and That Obtained with the oPE*n* Oligomers ($M_{w(oPEneq)}$)

a. SEC Results of the Oligomers

oligomers	M_w	V_e (mL)	$\bar{M}_{w(PSeq)}$	M_w/M_n	$\bar{L}_g$ (nm)
oPE1	340	18.22	1686	1.09	
oPE2	607	17.82	2246	1.02	1.2
oPE3	921	17.23	3427	1.02	1.9
oPE5	1550	16.58	5460	1.05	3.3
oPE7	2179	16.15	7432	1.09	4.7

b. Comparative Molecular Weights of Homo and Copolymers

polymers	V_e (mL)	$\bar{M}_{w(PSeq)}$	M_w/M_n	$\bar{M}_{w(oPEneq)}$	$\overline{DP}_w$	$\bar{L}_g$ (nm)
pPE*n*Bz	15.53	20 389	1.71	3880	13	8.6
pPE*n*Py	17.10	3762	1.21	1014	10	6.5
pPE*n*(Bz-*co*-Py)	16.73	14 506	2.96	1392	4	5.1
pPE*n*(Bz-*co*-Ti)	15.87	9083	2.17	2902	7	8.9
pPE*n*(Bz-*co*-Cz)	16.83	4565	1.42	1277	3	3.0

[a] The $\bar{L}_g$ represents the mean chain length from the calculated $\overline{DP}_w$.

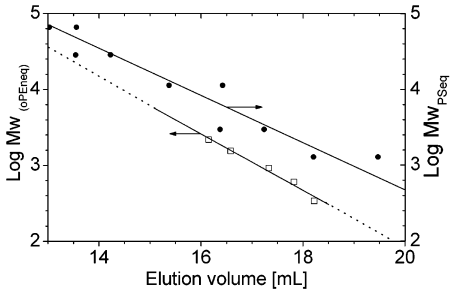

Figure 1. SEC calibration curves, line with black dots (●); PS calibration curve ($M_{w(PSeq)}$), line with open squares (□). Specific calibration curve from rigid benzoate ethynylene oligomers having 1, 2, 3, 5, and 7 repeat units ($M_{w(oPEneq)}$). THF as elution solvent at the rate of 1 mL/min.

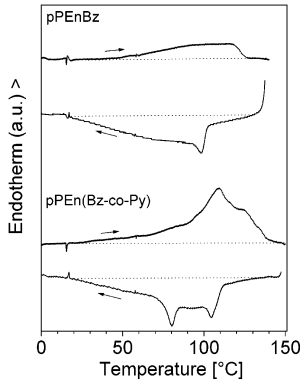

Figure 2. DSC of pPE*n*Bz and pPE*n*(Bz-*co*-Py). The second heating and cooling cycles were performed at scanning rates of 5 °C min^{-1} under nitrogen.

to an insoluble polymer fraction, which is formed during or after purification mainly by an aggregation phenomenon.[21]

2.2. Molecular Structure and Thermal Properties. By thermogravimetric analysis, the homo- and copolymers show a good stability in nitrogen or in air up to 180 °C, where the mass loss is less than 2%. The thermal properties are observed first by optical microscopy with polarized light. At room temperature, pPE*n*Bz or pPE*n*(Bz-*co*-Py) appears as a highly viscous and strongly birefringent paste. On heating the polymers become fluid at around 100 °C, and they remain birefringent until the beginning of decomposition around 180−200 °C. The birefringent textures of the two homopolymers are not typical of mesomorphic textures reported in the literature, making difficult the determination of the nature of the mesophases. As for copolymers, neither pPE*n*(Bz-*co*-Ti) nor pPE*n*(Bz-*co*-Cz) are birefringent at room temperature; they become fluid at 110 and 145 °C, respectively.

The thermal and structural behaviors of the polymers have been also studied by DSC and X-ray diffraction on powders. Figure 2 shows the thermograms for the second heating and cooling of pPE*n*Bz and pPE*n*(Bz-*co*-Py). For pPE*n*Bz, a broad endothermic transition is observed between 37 °C and 128 °C (ΔH = 14.8 J/g). On cooling, the thermogram is characterized also by a broad exothermic transition between 129 and 14 °C (ΔH = −15.9 J/g) with a peak at 98 °C. On heating, pPE*n*(Bz-*co*-Py) shows a large exothermic transition ranging from 30 to 140 °C (ΔH = 27.2 J/g) with a main peak at 109 °C and a shoulder at 124 °C. On cooling, two exothermic peaks are observed at 104 and 80 °C (total ΔH = −28.4 J/g). Indeed it is difficult to assign the enthalpic peaks

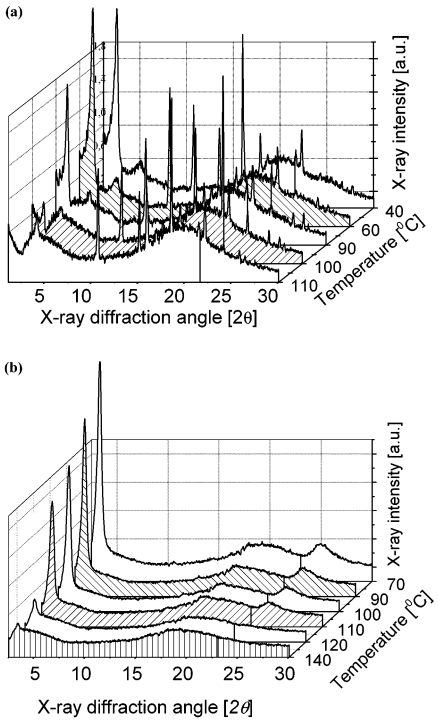

Figure 3. Temperature dependence of X-ray diffraction patterns for (a) pPE*n*Bz and (b) pPE*n*(Bz-*co*-Py) powders in the second heating. The relative X-ray intensities were normalized at $2\theta \sim 20°$.

to the fusion of the alkyl or aromatic parts for both polymers, *since* the $\pi-\pi$ interaction between the aryls is very strong, in particular for the copolymer that forms hydrogen bonds between the nitrogen and the alcohol group.

The X-ray diffraction of pPE*n*Bz (Figure 3a) at low temperature exhibits two sharp reflections in the low-angle region at $2\theta = 2.52°$, corresponding to reciprocal spacings of 3.5 ± 0.2 nm in the ratio 1:2, which are indicative of a lamellar system. In the wide-angle region, two broad bands (at $2\theta = 20.3$ and 24.3°), corresponding to spacings of 0.45 and 0.35 nm, are respectively attributed to the average spacing of the alkyl chains and to van der Waals interactions between phenyl rings. They are related respectively to a liquidlike order of the side chains within the lamellae and to a weak phenyl $\pi-\pi$ interaction between rigid cores. On heating, the peaks at small angles vanish, corresponding to the disappearance of the lamellar structure. However, sharp X-ray diffraction peaks superpose on these signals and indicate the presence of microcrystals. Therefore, pPEnBz appears to exhibit the coexistence of two phases consisted of a disordered LC phase and of microcrystals. In the LC phase, the layer spacing being twice the length of a repeat unit in an extended conformation, the molecules are arranged in a double layer with a comb like conformation (Figure 4a). Such a two-phase system may explain the very broad endothermic transition observed in DSC (see above).

The X-ray diffraction pattern of pPE*n*(Bz-*co*-Py) in Figure 3b, shows at small angles, a sharp reflection at 2θ = 3.25 corresponding to a lamellar system with spacing of 2.7 ± 0.2 nm. In the wide-angle region, two broad bands (at 20.16 and 25.30°) are observed, which were assigned to the alkyl spacers (here 0.45 nm) and to the aromatic interactions (0.36 nm), indicating a liquidlike order within the layers. All the patterns

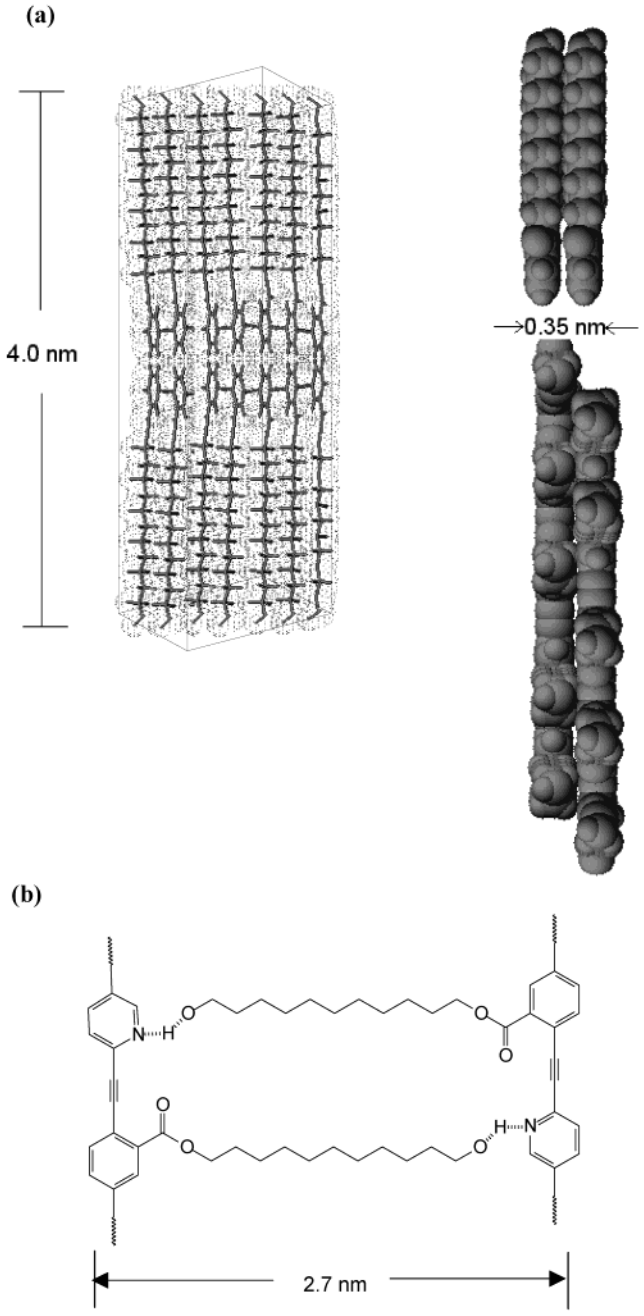

Figure 4. Molecular models deduced from X-ray diffraction powder: (a) for pPE*n*Bz, a three-dimensional view, a side view, and a top view respectively of the smectic-A mesophase arrangement; (b) for pPE*n*(Bz-*co*-Py), a view showing the hydrogen bond interactions between the lateral alcohol group and the pyridine moiety.

registered as a function of temperature are characteristic of a single LC phase. The 2.7 nm spacing suggests a *double layer structure with interdigitation* of the side chains. This period is consistent with the model depicted in Figure 4b. Moreover, the interdigitation allows the possible formation of hydrogen bonds between the OH group of the side chain and the nitrogen of the pyridine. For pPE*n*(Bz-*co*-Ti) and pPE*n*(Bz-*co*-Cz), the diffractograms are significantly different, as they reveal no periodic structure at low angle, while in the wide-angle region a diffuse broad band is observed. The diffractograms confirm the quasi-amorphous nature of such copolymers as observed by thermal and optical analysis. The lack of order of thiophene and carbazole copolymers

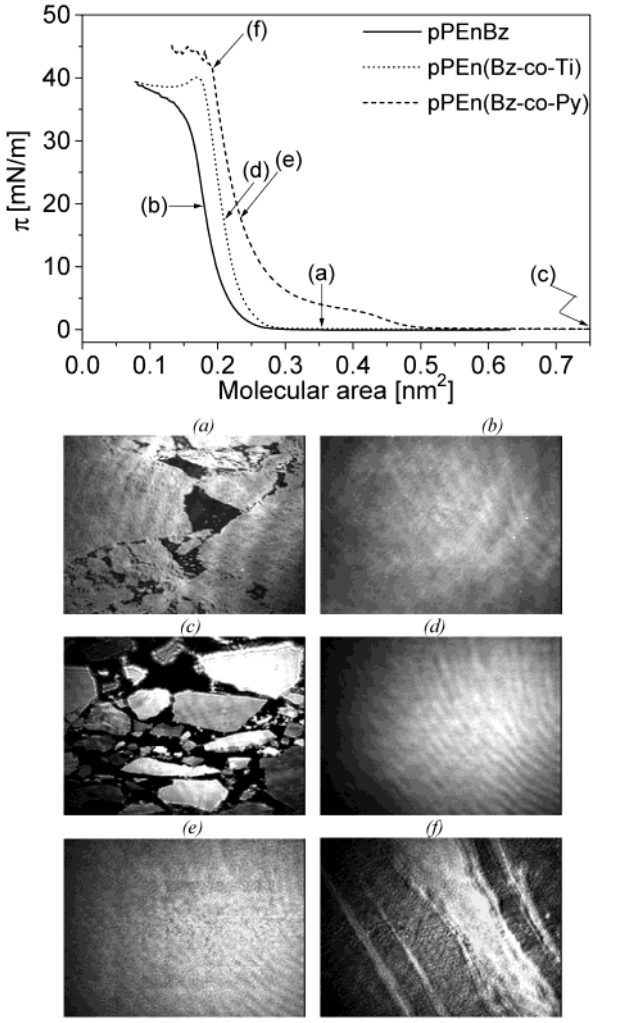

Figure 5. Pressure−area isotherms of the homo- and copolymers in Langmuir films at 30 °C and the related BAM pictures: (a, b) for pPE*n*Bz; (c, d) for pPE*n*(Bz-*co*-Ti); (e, f) for pPE*n*(Bz-*co*-Py). The pictures correspond to the surface pressure-molecular area/repeated unit: (a) ∼ 0 mN/m at 0.35 nm^2/repeated unit; (b) 20 mN/m, at 0.20 nm^2/repeated unit; (c) ∼ 0 mN/m at 0.85 nm^2/repeated unit; (d) 17 mN/m, at 0.21 nm^2/repeated unit; (e) 17 mN/m, at 0.21 nm^2/repeated unit; (f) 35 mN/m at the collapse pressure, respectively.

can be understood on the basis of the possible conformations of the main chain. According to the CPK models, the bond angles on the thiophene or carbazole unit with the ethynylene groups are 125 and 122°, respectively, giving rise to a statistic disorder.

2.3. Langmuir Films Characterization. All the polymers are amphiphilic enough to form stable Langmuir and Langmuir−Blodgett (LB) films. Figure 5 shows the pressure−area isotherm corresponding for pPE*n*Bz (continuous line), pPE*n*(Bz-*co*-Ti) (dotted line), and pPE*n*(Bz-*co*-Py) (dashed line). The pPE*n*Bz shows a liquid expanded behavior already observed on the oPE5 and oPE7 oligomers[7,11] with the same typical high compressibility at low pressures. At a molecular area close to 0.27 nm^2/repeated unit, the pressure levels up and the compressibility decreases. The isotherm is perfectly reversible after several compression−decompression cycles and no hysteresis is observed for surface pressures lower than 20 mN/m and temperatures higher than 30 °C. Figure 5, parts a and b, shows the Brewster angle microscopic (BAM) pictures at successive compression steps of the isotherm. The deposition of pPE*n*-

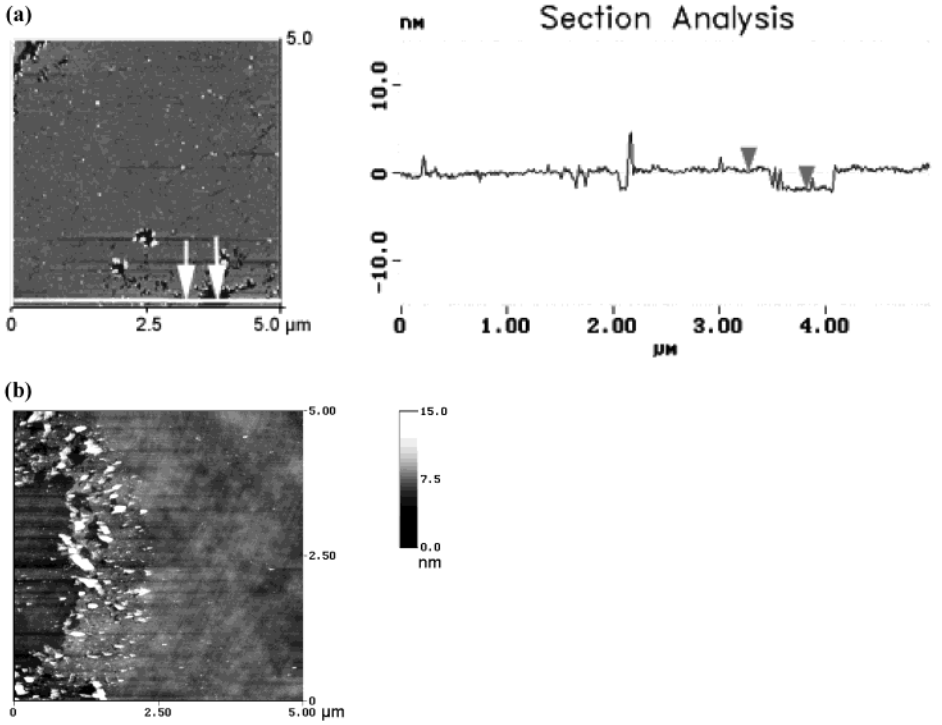

Figure 6. AFM images of a double LB layers on Si wafers: (a) pPE*n*(Bz-*co*-Py), the section analysis showing a single step defect of 2.8 ± 0.1 nm; (b) pPE*n*Bz, the image taken near one of the Si borders showing a step defect of 3.5 ± 0.02 nm. The scan was in tapping mode with a scanning rate of 0.39 Hz.

Bz solution has led to the coexistence of two bidimensional phases; isolated solid blocks randomly distributed in a gaseous phase. The coalescence of these blocks during compression (π between 15 and 20 mN/m) (Figure 5a) yields the disappearance of defects and the formation of a homogeneous film (Figure 5b). At this point, the specific molecular area, extrapolated at zero pressure, is $A_0 = 0.20 \pm 0.02$ nm^2/repeated unit, the same value than that was found for oPE7 ($A_0 \cong 0.21 \pm 0.02$ nm^2/repeated unit). An irreversible domain begins for a pressure higher than 20 mN/m, where the BAM shows an increase of defects, the molecular layer becoming more and more heterogeneous up to the collapse at pressure near 30 mN/m. During the decompression step, the film cracks forming solid blocks that will reassemble in the next compression cycle into a new homogeneous film.

For pPE*n*(Bz-*co*-Ti), the isotherm at 30 °C shows the same behavior than for pPE*n*Bz. At high molecular area, in the range 0.85−0.30 nm^2/repeated unit, isolated solid blocks are distributed in a homogeneous gas phase (Figure 5c). For pPE*n*(Bz-*co*-Py), the isotherm shows a gas−liquid-phase transition, which occurs at 0.51 nm^2/repeated unit and then, in the range 0.51−0.23 nm^2/repeated unit, a heterogeneous liquid expanded phase. The films of pPE*n*(Bz-*co*-Ti) and pPE*n*(Bz-*co*-Py) become homogeneous around 17 mN/m without any defect as observed by BAM (Figure 5, parts d and e). The molecular areas, extrapolated from the isotherms at zero pressure, are $A_0 = 0.23 \pm 0.07$ and 0.27 ± 0.07 nm^2/repeated unit for the Ti and Py copolymers, respectively. At lower areas, for the two copolymers the compressibility decreases and the pressure rises until the collapse is reached at 40 and 43 mN/m for the Ti and Py copolymers, respectively. Figure 5f shows a typical BAM image for the collapsed (Bz-*co*-Py) film. On the contrary, for pPE*n*(Bz-*co*-Cz), the Langmuir film is always characterized by the presence of solid blocks randomly distributed that never coalesce to form a homogeneous film.

2.4. Characterization of Langmuir−Blodgett Films. For pPE*n*Bz and copolymers, a good transfer of the Langmuir films onto substrates is possible *at temperatures close to 60 °C*. At lower temperatures, only fragments of films could be transferred, probably because of the too rigid properties of the monolayers. The transfer of the pPE*n*Bz LB film is studied on hydrophilic and hydrophobic substrates. Poor transfer ratios (TR < 0.3) are obtained on hydrophobic substrates, while on hydrophilic substrates, the transfer ratio reaches 0.98 ± 0.04. The transfers are only possible by lifting, which means that the multilayer presents an X-type molecular arrangement. Moreover drying at air for 2 or 3 h is required after every upstroke in order to get a well-structured multilayer film.

The transfer and deposition of pPE*n*(Bz-*co*-Ti) and pPE*n*(Bz-*co*-Py) LB films onto hydrophobic substrates were performed only by immersion-lifting cycle, favoring a Z-type molecular assembly. A good transfer ratio of 1.2 ± 0.3 is obtained for the first deposition on hydrophobic surfaces but it decreases slightly for the successive immersions. On the contrary, the transfers on hydrophilic substrates are only possible for the first layer with a TR of 1.3 ± 0.3. For the second and following transfers the TR decreases down to 0.5 ± 0.1, thus no stable multilayers of copolymers could be obtained on hydrophilic substrates. Figure 6a shows the AFM image of a transferred layer of pPE*n*(Bz-*co*-Py) on a wafer of hydrophilic silicon and its Z profile along the cross-section. The average roughness (R_q) is 0.35 nm for a surface of 6.25 μm^2 and an average height of the step of 2.8 ± 0.1 nm is measured. This value matches well with the thickness of a double layer according to the model proposed in Figure 4b. Similar thickness was found for a transferred layer of pPE*n*(Bz-*co*-Ti) on silicon, where the average height of the step is 2.9 ±

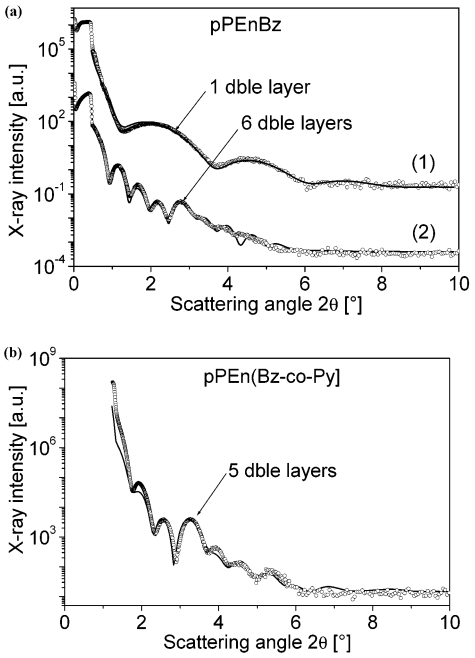

Figure 7. Grazing incidence X-ray reflectivity plots for (a) one (1) and six (2) double LB layers of pPE*n*Bz deposited on silicon wafer and ITO, respectively, and (b) five double and interdigitated LB layers of pPE*n*(Bz-*co*-Py) on ITO. The scattered points show the experimental data, and the continuous line shows the simulated reflectivity patterns obtained by GIXA.

0.02 nm, suggesting also a possible interdigitation of the alkyl chains giving place to double layer formations. The transferred layer surface of pPE*n*Bz on hydrophilic silicon is also quite flat, as observed in Figure 6b. The calculated roughness R_q is 0.8 and 0.32 nm for surfaces of 25 and 9.7 μm^2 respectively. A line scan on a defect near the border shows an average height of a step near 3.50 ± 0.02 nm, corresponding to a value that is consistent with a double layer thickness.

The grazing incidence X-ray scattering spectra corresponding to a double layer and a multilayer of pPE*n*Bz are reported in Figure 7a. The plot shows the X-ray intensity vs the scattering angle for one and six transferred layers respectively and the related GIXA simulated reflection patterns, which are represented as continuous lines. The Kiessig fringes as well as the Bragg peak are clearly visible in the experimental curves, which indicates that the transferred films are well structured. The Bragg peak at $2\theta = 2.3°$ on the multilayer (2) indicates a well-defined internal periodic electron density corresponding to a layered organization with a spacing of 3.3 nm, in agreement with the lamellar spacing determined already by X-ray diffraction on pPE*n*Bz powder (3.5 ± 0.02 nm). These results are likely consistent with the double layered organization on silicon (3.60 ± 0.05 nm) and the thickness determined on curve 1 by grazing incidence X-ray scattering (3.6 ± 0.5 nm) and by AFM (3.50 ± 0.02 nm). Nevertheless, these values do not match well with the periodicity calculated either from the Bragg peak in a multilayer film on ITO (3.3 ± 0.1 nm) or with a single layer model of molecules, where the side chains are in an extended conformation (2.0 nm). Hence, this result suggests a structural self-rearrangement in double layer, in a Y-type assembly with a slight tilt of the side chains within the LB film as found for the oPE7 oligomer.

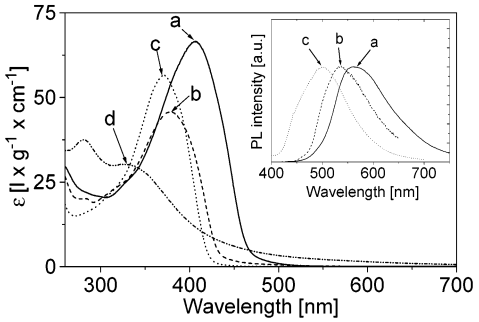

Figure 8. Optical absorption spectra in $CHCl_3$ solution corresponding to (a) pPE*n*(Bz-*co*-Ti), (b) pPE*n*Bz, (c) pPE*n*(Bz-*co*-Py), and (d) pPE*n*Py (in L g^{-1} cm^{-1}). The insert shows the normalized photoluminescence emission spectra in LB films of (a) pPE*n*(Bz-*co*-Ti), (b) pPE*n*Bz, and (c) pPE*n*(Bz-*co*-Py).

Figure 7b reports the experimental and the simulated diffraction pattern of pPE*n*(Bz-*co*-Py) for five transferred layers with a total thickness of 12.9 nm. For this copolymer, Kiessig fringes and Bragg peak are observed; they indicate a good periodic structure of the multilayer. The Bragg peak centered at $2\theta = 3.23°$ corresponds to a periodicity of 2.7 nm for the multilayer, while the thickness of a double layer is 2.8 nm. Furthermore, the 2.8 nm height found by AFM confirms that the molecular arrangement in the film is the same as in the mesomorphic phase characterized by X-ray diffraction, corresponding to the interdigitated alkyl chain self-assembly already described in Figure 4b. A similar result was observed for pPE*n*(Bz-*co*-Ti), where a thickness of 2.9 ± 0.3 nm corresponds also to a double and interdigitated layer. All the structural parameters of the different films are collected in Table 2. We attribute the good stability of the polymer layers on hydrophobic substrates to the presence of hydrogen bonds and also the $\pi-\pi$ interactions between the phenyl rings.

2.5. Photoluminescence and Electroluminescent Properties. Figure 8 shows the spectroscopic absorption of the polymer solutions of pPE*n*Bz, pPE*n*Py, pPE*n*(Bz-*co*-Py), pPE*n*(Bz-*co*-Ti), and pPE*n*(Bz-*co*-Cz) respectively, together with the PL emission spectra of their corresponding LB films (in insert). The optical properties are reported in Table 3. As expected from the electron charge transfer between the phenyl and thiophene as electron donor unit in pPE*n*(Bz-*co*-Ti), the excitonic peak is red-shifted from 404 to 412 nm with respect to the homopolymer pPE*n*Bz. For pyridine as the electron-acceptor unit in the copolymer pPE*n*(Bz-*co*-Py), the excitonic peak is blue shifted from 404 to 390 nm. This effect is also observed in the energy shift of the emission spectra. While the photoluminescence of pPE*n*Bz reaches a maximum of emission at 539 nm, the pPE*n*(Bz-*co*-Ti) copolymer is red shifted to 569 nm, and for the pPE*n*(Bz-*co*-Py) copolymer, the emission is blue shifted to 502 nm. The pPE*n*Py does not show any emission. The same behavior is also observed in the Raman spectra, where the −C≡C− stretching vibration energy centered at 2186, 2198, and 2206 cm^{-1} for pPE*n*(Bz-*co*-Ti), pPE*n*Bz, and pPE*n*(Bz-*co*-Py), respectively, moves to lower frequencies as a result of the increase in the π-electron delocalization of the conjugated backbone. From these results, it is clear that the electronic nature of the aryl group affects the conjugation and induces the photon modulation of these materials from the blue-green to the yellow region.

To prepare electroluminescent diodes, the photoluminescence quantum yield (Φ_{PL}) is measured as a

Table 2. Structural Parameters of the pPE*n*Bz Homopolymer and the pPE*n*(Bz-*co*-Py) and pPE*n*(Bz-*co*-Ti) Related Copolymers in LB Multilayers Determined by X-ray Reflectometry (GIXA)

sample	LB transfer	Bragg peak (nm)	calcd thickness from GIXA (nm)	av roughness (nm)
pPE*n*Bz/Si (Figure 7a)	1		3.6 ± 0.50	0.33 ± 0.04
pPE*n*Bz/ITO (Figure 7a)	6	3.3 ± 0.1	16.3 ± 0.1	0.65 ± 0.3
pPE*n*(Bz-*co*-Py)/Si	1		2.8 ± 0.2	0.34 ± 0.02
pPE*n*(Bz-*co*-Py)/Si (Figure 7b)	5	2.7	12.9	0.63 ± 0.01
pPE*n*(Bz-*co*-Ti)/Si	1		2.9 ± 0.3	0.35 ± 0.04

Table 3. Spectroscopic Data of the Homopolymers and Copolymers in $CHCl_3$ and in Thin Films, Where the Excitation Wavelength Is at the Maximum of the Absorption Bands

EL material	λ_{max}(abs, $CHCl_3$) (nm)	ϵ (L g^{-1} cm^{-1})	λ_{max}(abs, film) (nm)	λ_{max}(PL, film) (nm)	Φ_{PL} (%)[a]	λ_{max}(EL) (nm)
pPE*n*Bz[a]	380	46.9	404	539	23	555
pPPE*n*Py	327	30.4	362	no		
pPE*n*(Bz-*co*-Py)	371	56.5	390	502	15	550
pPE*n*(Bz-*co*-Ti)	405	66.53	412	569	12	
pPE*n*(Bz-*co*-Cz)	378	45.2	404	563	7	
oPE7[a]	374	56.5	382	516	19	527
oPE5[a]	364	50.3	374	504	24	

[a] Films deposited by spin coating; the total thickness is in the range of 250−300 nm.

Table 4. Fluorescence Quantum Yields (Φ_{PL}, %) and Absorption Coefficient (*A*) of Phenyl−Ethynylene Oligomers and Polymers Measured by the Integration Sphere Method, on the LB and Spin-Coated Films vs the Thickness[a]

a. LB Films

oPE7	1 LB layer	4 LB layers	8 LB layers	spin-coated film
thickness (nm)	3.7	14.8	29.6	300.0
Φ_{PL} (%)	9.0	16.0	20.0	19.0
A	0.08	0.23	0.37	0.85

b. Spin-Coated Films

polymer	pPE*n*Bz coated film	Bz-*co*-Ti 2 LB layers	Bz-*co*-Ti coated film	Bz-*co*-Py 2 LB layers	Bz-*co*-Py coated film	Bz-*co*-Cz coated film
Φ_{PL} (%)[b]	23.0	3.0	12.0	11.0	15.0	7.0
A	0.77	0.33	0.65	0.16	0.74	0.09

[a] The excitation wavelength for the fluorescence quantum yields is at 411 nm. [b] The thickness of all spin-coated films is in the range 250−300 nm

function of the film thickness for the polymers including different heteroatoms. Table 4, parts a and b, reports the results of Φ_{PL} and the absorption coefficient (*A*) for the different oligomers and polymers. As a comparative study, different numbers of oPE7 LB layers showed that the PL yield is directly affected by the film thickness. A maximum Φ_{PL} is given for films having eight double layers with a total thickness of 29.6 nm. For higher thickness a *clear decrease of yielding is observed*; i.e., for a spin-coated film of 300 nm, the Φ_{PL} is 19%. This is consistent with the increase of the absorption coefficient (*A*) with thickness. Similar results are found by Paloheimo et al.,[22] who found the highest Φ_{PL} for films having nine LB layers of thiophene oligomers. Thus, work is now in progress on LED's by taking into account the LB layers number. Another factor that affects the Φ_{PL} is the heteroatoms such as O, S, and N. While for pPE*n*Bz films Φ_{PL} is about 23%, the copolymers in the series Py, Ti, and Cz show markedly lower photoluminescence yields downward to 15, 12 and 7% respectively.

To check if a well-ordered arrangement of the conjugated chains has been induced through the LB process, the anisotropic optical properties have been investigated. A rather good dichroism has been found in absorption (R = 2.0, 2.04 and 1.3) and in emission (R = 3.4, 4.0 and 2.6) spectra for pPE*n*Bz, pPE*n*(Bz-*co*-Ti), and pPE*n*(Bz-*co*-Py), respectively. These properties highlight the emission dichroic ratio, which always presents higher values than in absorption. This phenomenon, which has been already observed by Neher[23] and Chen,[24] was ascribed to the possible energy transfer that can take place after excitation in the domains of well-aligned molecules. However, it has not been well elucidated yet.

Recently we reported that oPE7 oligomer containing the (11-undecanol) benzoate moiety is an electroluminescent material operating at low voltages (4.5−6.0 V) in LED devices. Moreover, a rubbing process of the films allowed to obtain polarized electroluminescence.[12] In the present work, we investigate the inherent electroluminescent properties of the corresponding series of homo- and copolymers. Hence, two devices were prepared by spin coating pPE*n*Bz and pPE*n*(Bz-*co*-Py) to obtain 550 and 300 nm thick films, respectively. We did not try to optimize the diode performances with regard to the film thickness, the film morphology, or the charge injection process. Under voltage bias in the forward direction, the two diodes of pPE*n*Bz and pPE*n*(Bz-*co*-Py) show a yellow and blue-green emission at *low threshold voltages* of 3.8 and 4.2 V, respectively. The luminescence−voltage and the current density−voltage characteristics are displayed in Figure 9. The two plots show a typical diode behavior where the current follows well the luminescence *due to the orientation of internal dipoles as suggested by Zou et al.*[25] With increasing forward voltage, both the current density and the emitting light intensity increase rapidly after 3.8 and 4.2 V. However, a marked difference on EL intensity saturation is seen between the two diodes. For pPE*n*Bz the LED reaches a maximum irradiance of about 3.2 μW cm^{-2} at typical

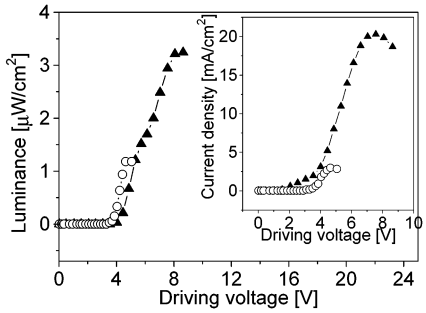

Figure 9. Luminance−voltage plot of the (ITO/Film/LiF−Al) LEDs of pPE*n*(Bz-*co*-Py) (circles) and pPE*n*Bz (triangles). The insert figure shows the current density−voltage behavior for the two related diodes.

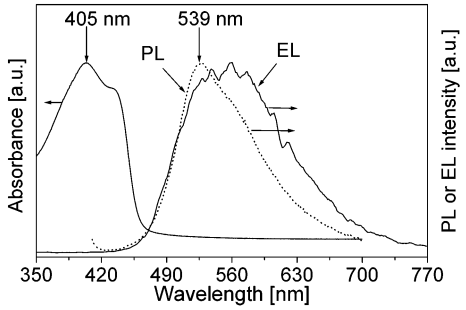

Figure 10. Normalized absorption, photoluminescence (PL), and electroluminescence (EL) spectra of a spin-coated film of pPE*n*Bz. The emission intensity of the LED is measured in a (ITO/film/LiF−Al) device.

currents of 20 mA cm^{-2}. For a pPE*n*(Bz-*co*-Py) device, the corresponding values are 1.2 μW cm^{-2} and 2.8 mA cm^{-2}, respectively. Even if these last emission properties are too low to justify a direct application of this material, it points out that pPE*n*(Bz-*co*-Py) can be used as an efficient holes transport layer by the fact that pyridine is a good electron acceptor. The EL spectrum of pPE*n*Bz is represented in Figure 10. The maximum emission is centered at 555 nm, 14 nm red-shifted with respect to the maximum emission of the PL spectra at 539 nm. This shift of the emission peak can be attributed to a localized recombination of the charges close to one of the electrodes. The calculated corresponding external quantum efficiency was close to 10^{-5} % photon per injected electron.

3. Conclusions

In conclusion, we report in the present work, the synthesis, the structural and optical properties of new poly(phenyl−ethynylenes), pPE*n*Bz, pPE*n*Py, and the related copolymers pPE*n*(Bz-*co*-Ti), pPE*n*(Bz-*co*-Py), and pPE*n*(Bz-*co*-Cz). All these polymers give films of good optical quality by spin coating or by LB film deposition techniques. The different conformations of the polymer chains induced by the alkyl-substituted phenyls lead to specific supramolecular assembly of the molecules in the films. The homopolymer benzoate and the copolymers have been processed into materials showing a photoemission in the range of blue-green to yellow. Such films can be applied as active layers in electroluminescent diodes. Preliminary results of LEDs based on pPE*n*(Bz-*co*-Py) suggest also the possibility of using the copolymer as holes transport material in order to increase the electroluminescent yields. The polarized photoluminescence observed on polymers from oriented LB films is also very important for the future realization of more sophisticated devices with further enhanced brightness, polarized emission, and improved light efficiency.

4. Experimental Section

4.1. Materials. The following chemical reactives, palladium chloride ($PdCl_2$), triphenylphosphine (TPP), copper(I) iodine (CuI), trimethylsilylacetylene (TMSA), 2,5-dibromobenzoic acid, 11-bromo-1-undecanol, 1,5-diazabicyclo[4.3.0]non-5-ene (DBN), tetrabutylammonium fluoride in THF (TBAF) 2,5-dibromopyridine, 3,6-dibromocarbazole, and 2,5-dibromothiophene, were obtained from Aldrich and Lancaster. CH_2Cl_2, $CHCl_3$, C_6H_6, methanol and THF were purchased from Prolabo. Dry triethylamine was obtained by vacuum transfer from KOH. All the chemical materials were used without further purification.

4.2. Synthesis of Homo- and Copolymers. The monomer diethynyl benzoate was synthesized by using the following pathway:

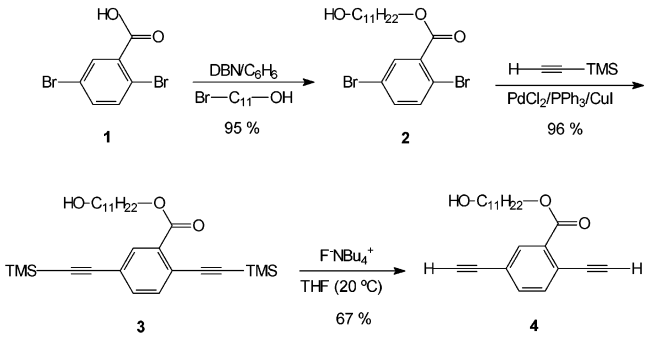

Synthesis of (11-Undecanol) 2,5-Dibromobenzoate (2). A round-bottom flask was charged with 2,5-dibromobenzoic acid (12 mmol, 3.360 g), 11-bromo-1-undecanol (12 mmol, 3.012 g) and benzene (40 mL). The mixture was heated at 85 °C and stirred until total product dissolution. Later, DBN (12 mmol, 1.48 mL) was added. The mixture was refluxed overnight, and after cooling, water (100 mL) was added. The mixture was transferred to a separated funnel and the organic layer extracted with benzene and dried with $MgSO_4$. After filtering off the drying agent, the solvent was removed under vacuum and the crude product was chromatographied through a silica gel column using CH_2Cl_2/CH_3OH, (1 L/4 mL) as eluent to afford a pale yellow powder (**2**). Mp: 59−62 °C. ^1H NMR (200 MHz, $CDCl_3$): δ (ppm) 7.9(d, 1H, −PhH), 7.53 (d, 1H, −PhH), 7.46 (dd, 1H, −PhH), 4.34 (t, 2H, $-COOCH_2-$), 3.65 (t, 2H, $-CH_2$-OH), 1.78(q, 2H, $-CH_2-\beta$-COO), 1.59(q, 2H, $-CH_2-\beta$-OH), 1.30 (m, 14H, $-CH_2-$). Anal. Calcd for $C_{18}H_{26}Br_2O_3$: C, 48.01; H, 5.82; O, 10.66. Found: C, 48.40; H, 5.89; O, 10.31.

Synthesis of (11-Undecanol) [2,5-Bis((trimethylsilyl)-ethynylene)]benzoate (3). A two-neck round-bottomed flask containing previously degassed triethylamine (100 mL) was charged with $PdCl_2$ (0.88 mmol, 0.156 g), CuI (0.44 mmol, 0.083 g), and TPP (3.96 mmol, 1.03 g) under argon. The mixture was heated at 80−85 °C for 20 min. Then, **(2)** (8.8 mmol, 4 g) was added and stirred vigorously for 10 min. Finally, TMSA (22 mmol, 3.1 mL) was added via cannula in one step and stirred for 16 h. After cooling, the mixture was washed with a saturated solution of ammonium chloride. The organic phase was extracted with diethyl ether (2 × 100 mL), washed twice with distilled water, and dried with $MgSO_4$. After solvent evaporation, the viscous syrup was passed through a silica gel column using CH_2Cl_2/THF, (75/25 v/v) as eluent to obtain a brown oil (**3**). ^1H NMR (200 MHz, $CDCl_3$): δ (ppm) 7.98 (d, 1H, −PhH), 7.51 (s, 2H, −PhH), 4.32 (t, 2H, $-COOCH_2-$), 3.64 (t, 2H, $-CH_2OH$), 1.78(q, 2H, $-CH_2-\beta$-COO), 1.59(q, 2H, $-CH_2-\beta$-OH), 1.30 (m, 14H, $-CH_2-$), 0.26 (s, 18H, $SiCH_3$). Anal. Calcd for $C_{28}H_{44}O_3Si_2$: C, 69.36; H, 9.19; O, 9.90. Found: C, 69.12; H, 9.17; O, 10.5.

Synthesis of (11-Undecanol) 2,5-Diethynylbenzoate[6] (4). A round-bottom flask charged with **(3)** (7.2 mmol, 3.51 g) and wet THF (100 mL) was cooled to −20 °C. Then a 1 M

solution of TBAF (2 mmol, 2 mL) was added, and the reaction was stirred for 5 s and then stopped by passing the reaction mixture through a plug of silica gel. The crude product was chromatographied using CH_2Cl_2/ THF (90/10 v/v) as eluent to obtain a red viscous liquid. ^{1}H NMR (200 MHz, $CDCl_3$): δ (ppm) 8.05 (s, 1H, −PhH), 7.57 (s, 2H, −PhH), 4.34 (t, 2H, $-COOCH_2-$), 3.64 (t, 2H, $-CH_2OH$), 3.48 (s, 1H, −C≡CH), 3.22 (s, 1H, −HC≡C−), 1.76(q, 2H, $-CH_2-\beta$-COO), 1.58(q, 2H, $-CH_2-\beta$-OH), 1.30 (m, 14H, $-CH_2-$). Anal. Calcd for $C_{22}H_{28}O_3$: C, 77.64; H, 8.23; O, 14.13. Found: C, 77.41; H, 8.34; O, 14.54.

Polymerization of homo- and copolymers was achieved by a Pd/Cu cross-coupling reaction.[26−28]

A typical procedure is described as follows: A two-neck round-bottomed flask containing previously degassed and dried triethylamine (100 mL) was charged with $PdCl_2$ (0.145 mmol, 26 mg), CuI (0.072 mmol, 14 mg), and TPP (0.432 mmol, 114 mg) under argon. The mixture was heated at 80−85 °C for 20 min. Then, the dibromoaryl was added: (11-undecanol) 2,5-dibromobenzoate (1.45 mmol, 648 mg) or 2,5-dibromopyridine or 3,6-dibromocarbazole or 2,5-dibromothiophene and the mixture stirred vigorously for 10 min. Finally, (11-undecanol) 2,5-diethynylbenzoate (1.45 mmol, 490 mg) was added via a cannula in one step and stirred overnight. After cooling, the mixture was filtered off to eliminate the ammonium salt formed and the organic phase was partially evaporated and washed with a saturated solution of sodium diethyldithiocarbamate.[29] The organic phase was extracted with chloroform and washed twice with distilled water and the solvent removed. The pasty residue was dissolved in 6 mL of chloroform and poured into 50 mL of cold methanol to precipitate and then centrifuged. The product was recuperated in 5 mL of chloroform yielding between 80 and 90%. All the optical characteristics are collected in Table 3. The homopolymers and copolymers were purified from residual monomers and shortest oligomers by *preparative size exclusion chromatography*. They were characterized by ^{1}H and ^{13}C NMR as well as by elemental analysis.[30]

4.3. Instruments and Methods. Macromolecular Characterization. SEC has been performed on a Waters chromatograph using a refractive index detector and THF as effluent at 1 mL/min. The thermogravimetric analysis has been carried out on a Mettler TA 300. Differential scanning calorimetry was performed on a Perkin-Elmer DSC 7 at a rate of 5 °C/min for both the heating and cooling cycles. The X-ray diffraction study has been realized on a Debye−Scherrer-type chamber with 900 nm of circumference and equipped with a Mettler FP52 heating stage. The rotating anode and generator were from Marconi-Avionics.

^{1}H and ^{13}C NMR data were obtained at room temperature with a Brüker AC-200F (200 MHz) spectrometer using $CDCl_3$ as chemical shift standard.

Spectroscopic Characterization. UV−visible absorption spectra were measured in $CHCl_3$ and in casting and LB films using a Hitachi U-3000 spectrophotometer equipped with polarizers. The chain orientation was evaluated by the dichroic ratio, $R = A_{\parallel}/A_{\perp}$ where $A_{\parallel}$ and $A_{\perp}$ are the absorbance in parallel and normal polarization of light relative to the dipping direction. The emission spectra have been obtained with a PTI C60-1717 spectrofluorimeter from Photon Technology International. Raman scattering measurements were made with a 1064 nm Nd:YAG laser line and the diffused intensities were detected on a Brücker FTIR spectrometer IFS 66.

Langmuir and Langmuir—Blodgett Films. Solutions were prepared using $CHCl_3$ (Analysis Grade, Carlo Erba) at 2−2.5 mg/mL concentrations. Volumes of 10 to 60μL were spread using a microsyringe. Spreading solutions were left 15 to 20 min to equilibrate before the compression started. Data were collected with a KSV LB5000 system (KSV Instruments) using a symmetrical compression Teflon barrier in a clean dust free environment. The trough temperature was controlled to ±0.1 °C. The ultrapure water (ρ = 18.2 MΩ.cm) used for the subphase was obtained from a Milli-RO3-plus and Milli-Q185 ultrapurification system from Millipore. The Wilhelmy plate method (platinum) was used for surface pressure measurements. The monolayers were compressed with a typical speed of 10.5 and 1.5 mm/min for the pPE*n*Bz, pPE*n*(Bz-*co*-Ti) and pPE*n*(Bz-*co*-Py), respectively. Isotherms were reproducible from run to run and showed no noticeable hysteresis. LB films of pPE*n*Bz were obtained by transfer only on hydrophilic glass slides, ITO, and silicon wafers (100) at surface pressures ranging from 18 to 20 mNm^{-1}. Transfers on substrates started always from below the surface with a lifting speed of 3 mm/min. On the other hand, Ti and Py copolymers were only transferred on hydrophobic substrates and the substrates themselves started from above the surface with a down speed of 2 and 1.5 mm/min, respectively.

Hydrophilic Surfaces. Prior to transfer, glass substrates were cleaned using the following procedure: the plates were immersed in a hot detergent solution (Decon 90, 4% v/v) over 5 h and rinsed 10 times with hot water, or were treated by a hot sulfochromic solution and rinsed with ultrapure water in an ultrasonic bath over 20 min, and then dried in nitrogen flux and heated at 50 °C. Si substrates were treated according to a modified RCA procedure.[31]

Hydrophobic Surfaces (OTS Preparation, Sagiv[32] Method). The glass substrates and the Si wafers were first treated following the same procedure used to have hydrophilic surfaces (described above). Then they were rinsed with water or ethylic alcohol and treated with an octadecyltrichlorosilane (OTS) solution (2% in heptane) in an ultrasonic bath for 10 min at 60−80 °C. Finally, the substrates were rinsed successively with chloroform and heated in an oven for 3 h at 120 °C.

Films Characterization. The grazing incidence X-ray studies of LB films were performed on a X′PERT-MPD apparatus from Philips, (with nickel β filter, programmable divergence slit ($^1/_{32}$°), parallel plate collimator, flat Ge monochromator, and a Xe detector). A Cu Kα beam at wavelength of 0.1542 nm was used. All measurements have been recorded immediately after the LB transfers. Data were analyzed by using GIXA (V2.1) software from Philips Electronics Instrument.

The AFM measurements were carried out with a Dimension 3100 from Digital Instruments operating at ambient atmosphere. The images were recorded at room temperature using the tapping mode at resonance frequency of 290−420 kHz. From the AFM recorded images, the roughness of the surface topography was characterized applying the standard deviation of the height values, denoted R_q, and obtained as follows: $R_q = [(1/N)\sum_i(Z_i - Z_m)^2]^{1/2}$, for i from 1 to N, where Z_m is the average of the Z values within the given image, Z_i is the current Z value and N is the number of points of the image.

Photoluminescence Quantum Yields. Φ_{PL} was measured in solid films using an integrating sphere (TRC-060-SL from Labsphere) and a laser excitation at 411 nm (PPm04 from Power Technology). The integrating sphere is a hollow sphere, coated inside with a diffusely reflecting material. The flux received at an aperture in the sphere (the exit port) is proportional to the total amount of light within the sphere, irrespective of its angular distribution. The samples were measured under pure nitrogen atmosphere, and Φ_{PL} was calculated by taking into account the incident light absorbed directly by the polymer film and after internal reflection.[33]

Electroluminescent Devices. Electroluminescent diodes were constructed with spin-coated films of pPE*n*(Bz-*co*-Py) from chloroform solutions and sandwiched between two electrodes (ITO/Film/LiF−Al).[34] The film deposited on top of ITO (15 Ω/cm^2) was previously dried for 12 h in a 10^{-7} mb vacuum chamber. The layer thickness of spin-coated and LB films were always determined by X-ray reflectivity and checked by a profilemeter DEKTAK 3. A LiF/Al cathode then covered the film as an electron injection.[35] The thickness of these evaporated layers, controlled by the quartz balance monitor was of 1.5 and 100 nm, respectively. The analyzed area of the EL devices was 0.33 cm^2. Diodes were studied in air, electroluminescence and photoluminescence spectra being recorded with a broadband Jobin-Yvon spectrometer coupled to an amplified Hamamatsu-CCD multichanel detector and with a F 4500-Hitachi fluorescence spectrophotometer, respectively.

Emitting light was measured with a calibrated 1 cm^2 area silicon photodiode (Hamamatsu) placed in front of the device and recorded by computer.

Acknowledgment. We wish to acknowledge the Mexican National Council for Science and Technology through the program CONACyT/SFERE for Scholarship 112097 to E.A.-M. and the CNRS through the GDR "Matériaux pour l'Optique nonlinéaire" (GDR 1181) for financial support for LED characterizations.

Supporting Information Available: Figures showing ^1H and ^{13}C NMR spectra and text giving experimental ^{13}C NMR data and elemental analyses. This material is available free of charge via the Internet at http://pubs.acs.org.

References and Notes

(1) Burroughes, J. H.; Bradley, D. D. C.; Brown, A. R.; Marks, R. N.; Friend, R.H.; Burns, P. L.; Holmes, A. A. B. *Nature (London)* **1990**, *347*, 539, Braun, D.; Heeger, A. J. *Appl. Phys. Lett.* **1991**, *58*, 1982. Yang, Y.; Heeger, A. J. *Nature* **1994**, *372*, 344. Hide, F.; DÍaz-GarcÍa, M. A.; Schwartz, B. J.; Heeger, A. J. *Acc. Chem. Res.* **1997**, *30*, 430.
(2) Thakur, M.; Frye, R.; Greene, B. *Appl. Phys. Lett.* **1990**, *56*, 1213.
(3) Townsend, P. D.; Baker, G. L.; Schlotter, N. E.; Klauser, C. F.; Etemad, S. *Appl. Phys.* **1988**, *53*, 1782.
(4) Zhou, Q.; Swager, T. *J. Am. Chem. Soc.* **1995**, *117*, 12593.
(5) Swanson, L. S.; Shinar, J.; Ding, Y. W.; Barton, T. J. *Synth. Met.* **1993**, *55*, 1.
(6) Yoshino, K.; Tada,; Onoda, K. M. *Jpn. J. Appl. Phys.* **1994**, *33*, L1785.
(7) Arias-Marin, E.; Arnault, J. C.; Guillon, D.; Maillou, T.; Le Moigne, J.; Geffroy, B.; Nunzi, J. M. *Langmuir* **2000**, *16*, 4309.
(8) Maillou, T.; Le Moigne, J.; Geffroy, B.; Lorin, A.; Rosilio, A.; Dumarcher, V.; Rocha, L.; Denis, C.; Fiorini, C.; Nunzi, J. M. *Synth. Met.* **2001**, *124*, 87.
(9) Berggren, M.; Inganäs, O.; Gustafsson, G.; Gustafsson-Carlberg, J. C.; Rasmusson, J.; Andersson, M. R.; Hjertberg, T.; Wennerström, O. *Nature* **1994**, *372*, 444.
(10) Rhenan, M.; Schulter, A. D.; Wegner, G. *Polymer* **1989**, *30*, 1054.
(11) Kim, J.; Swager, T. M. *Nature (London)* **2001**, *411*, 1030.
(12) Grell, M.; Bradley, D. D. C. *Adv. Mater.* **1999**, *11*, 895.
(13) Dyreklev, P.; Breggren, M.; Inganäs, O.; Anderson M. R.; Wennerström, O.; Hjertberg, T. *Adv. Mater.* **1995**, *7*, 43.
(14) Arias-Marin, E.; Arnault, J. C.; Guillon, D.; Maillou, T.; Le Moigne, J.; Geffroy, B.; Nunzi, J. M. *Mater. Res. Soc. Symp. Proc.* **2000**, *598*, BB1.8.1.
(15) Arias, E.; Maillou, T.; Moggio, I.; Guillon, D.; Le Moigne, J.; Geffroy, B. *Synth. Met.* **2002**, *127*, 229.
(16) Moroni, M.; Le Moigne, J.; Luzzati, S. *Macromolecules* **1994**, *27*, 562.
(17) Arias, E. *Ph.D. Thesis* **2000**, Université Louis Pasteur, Strasbourg, France.
(18) Giesa, R. *Rev. Macromol. Chem. Phys.* **1996**, *C36*, 671.
(19) Pearson, D. L.; Schumm, J. S.; Tour, J. M. *Macromolecules* **1994**, *27*, 2348.
(20) Sanechika, K.; Yamamoto, T.; Yamamoto, A. *Bull. Chem. Soc. Jpn.* **1984**, *57*, 752.
(21) Halkyard, C. E.; Rampey, M. E.; Kloppenburg, L.; Studer-Martinez, S. L.; Bunz U. H. F. *Macromolecules* **1998**, *31*, 8655.
(22) Pal, A. J.; Paloheimo, J.; Stubb, H. *Appl. Phys. Lett.* **1995**, *67*, 3909.
(23) Cimrova, V.; Remmers, M.; Neher, D.; Wegner, G. *Adv. Mater.* **1996**, *8*, 146.
(24) Chen, X. L.; Bao, Z.; Sapjeta, B. J.; Lovinger, A. J.; Crone, B. *Adv. Mater.* **2000**, *5*, 344.
(25) Zou, D.; Yahiro, M.; Tsutsui, T. *Jpn. J. Appl. Phys.* **1998**, *37*, L1406.
(26) Dieck, H. A,; Heck, R. F. *J. Organomet. Chem.* **1975**, *93*, 259.
(27) Heck, R. F. *Palladium Reagent in Organic Syntheses;* Academic Press: New York, 1990.
(28) Amatore, C.; Lutand, A.; Suarez, A. *J. Am. Chem. Soc.* **1993**, *115*, 9531.
(29) Bharathi, P.; Patel, U.; Kawaguchi, T.; Pesak, D. J.; Moore, J. S. *Macromolecules* **1995**, *28*, 5955.
(30) See paragraph at the end of the paper for Supporting Information available.
(31) Kern, W.; Puotinen, D. *RCA Rev.* **1970**, *31*, 187. Oxidative treatment: the substrates were soaked in a hot mixture of H_2O:H_2O_2:NH_4OH (or HNO_3) (40:30:30)% for 20 min and then rinsed in an ultrasonic bath with ultrapure water.
(32) Netzer, L.; Sagiv, L. *J. Electochem. Soc.* **1983**, *105*, 674.
(33) Greenham, N. C.; Samuel, I. D. W.; Hayes, G. R.; Phillips, R. T.; Kessener, Y. A. R. R.; Moratti, S. C.; Holmes, A. B.; Friend, R. H. *Chem. Phys. Lett.* **1995**, *241*, 89.
(34) Gautier, E.; Nunzi, J. M.; Sentein, C.; Lorin, A.; Raimond, P. *Synth. Met.* **1996**, *81*, 197.
(35) Hung, L. S.; Tang, C. W.; Mason, M. G. *Appl. Phys. Lett.* **1997**, *70*, 152.

MA020121E